Superelastic and inelastic He^{2+} + He state-selective electron capture

V. D. Irby,* T. J. Gay,† J. T. Park, S. W. Bross, and A. D. Gaus

Physics Department and Laboratory for Atomic and Molecular Research, University of Missouri–Rolla, Rolla, Missouri 65401

Experimental studies have been made of superelastic and inelastic collision processes involved in the state-selective single-electron capture reaction $^3He^{2+} + He(1\,^1S) \rightarrow {}^3He^+(n) + He^+(n')$, where n and n' are the final principal quantum-number states of the collision products. Total cross sections have been measured at projectile energies of 15, 30, and 45 keV/u, by examining the energy loss-gain of the fast $^3He^+$ product ions, for the superelastic $n = n' = 1$ channel, and for the sum of the inelastic $n = 2$, $n' = 1$ and $n = 1$, $n' = 2$ states. Measurements are also presented for Ne and Ar targets.

I. INTRODUCTION

The University of Missouri–Rolla Ion Energy Loss Spectrometer (UMRIELS) has been modified to study state-selective electron-capture reactions for bare ions incident on atomic or molecular targets. The main goal of these modifications is to study the reaction

$$He^{2+} + H, D \rightarrow He^+(n) + H^+, D^+ , \qquad (1)$$

which has been proposed as a diagnostic tool for fusion-plasma research [1]. Total cross sections for specific n (> 1) values in this reaction can be obtained by observing the line radiation emitted from the He^+ excited states, or from the energy loss-gain of the He^+ product ion. (Cross sections for $n = 1$ must be obtained using the latter method.) Energy loss-gain measurements have two distinct advantages over photon detection. First, cascading corrections are avoided because the fast collision partner is detected, rather than a secondary photon. Second, no knowledge of detector efficiencies is required because population ratios of specific n levels can be obtained directly from energy loss-gain spectra and can be put on an absolute scale by normalizing to existing experimental data for capture into all n levels. In contrast, the efficiency of photon detectors depends strongly upon the wavelength of the observed photon. Thus two sources of possible systematic error in the determination of final cross sections are eliminated with the energy loss-gain method.

As initially developed, the UMRIELS could be used to study only those collisions in which the initial and final charge states of the projectile were equal. In order to study collisions like (1), it was thus necessary to modify the existing apparatus [2–5] by adding a precision

voltage-divider circuit [6,7]. The operation of the apparatus with these modifications has been described in detail in Refs. [6] and [7].

In order to develop the techniques and technology needed to study collision (1) without the further experimental problems associated with a hydrogen target, our first studies, reported here, have investigated state-selective capture by $^3He^{2+}$ from He targets:

$$^3He^{2+} + He \rightarrow {}^3He^+(n) + He^+(n') . \qquad (2)$$

Here n and n' represent the final principle quantum numbers of the projectile and target states, respectively. Though the target species in reaction (2) is different from reaction (1), these respective collisions involve much of the same physics.

Extensive measurements have been carried out for total single capture cross sections for reaction (2) summed over all n and n' states:

$$He^{2+} + He \rightarrow He^+(\Sigma n) + He^+(\Sigma n') . \qquad (3)$$

Experimental data from the work of Shah, McCallion, and Gilbody [8], and the work of Dubois [9], exhibit a maximum value of 8×10^{-16} cm^2 at an incident projectile energy near 30 keV/u. Another important process that can occur in collisions of He nuclei with He is "transfer ionization" (TI):

$$He^{2+} + He \rightarrow He^+(\Sigma n) + He^{2+} + e^- , \qquad (4)$$

in which one electron is transferred to the projectile and the remaining electron is removed to the continuum leaving the target stripped of electrons. In order to extract total state-selective capture cross sections for this system, the energy loss-gain spectrum obtained must be integrated over all $^3He^+$ ion energies and angles, and normalized to the sum of the cross sections for reactions (3) and (4). This is because in making an energy loss-gain measurement on the fast $^3He^+$ ions in reaction (2), we cannot discriminate between reactions (3) and (4).

The only experimental data we are aware of that exist for state-selective electron capture in the intermediate (10–50 keV) energy range for reaction (2) were obtained

---

*Present address: Department of Physics and Astronomy, University of Kentucky, Lexington, KY 40506-0055.
†Present address: Behlen Laboratory of Physics, University of Nebraska, Lincoln, NE 68588.

in 1978 by Afrosimov *et al.* [10]. Their experimental method involved energy loss-gain measurements. Due to the resolution of their parallel-plate ion-energy analyzer the data are limited to energies below 50 keV. The high-energy-resolution capabilities of the UMRIELS have allowed us to make measurements of reaction (2) for projectile energies above 50 keV, ranging up to 135 keV.

II. EXPERIMENTAL APPARATUS

The modified University of Missouri–Rolla Ion Energy Loss Spectrometer consists of a 15–200 kV variable-angle ion accelerator, scattering chamber housing, switching magnet, deceleration optics, and either a cylindrical or retarding-field ion-energy analyzer. In order to study reactions in which the projectile-charge changes during the collision, a high-voltage, 10-GΩ, variable-resistor assembly (VRA) has been placed between the accelerator and decelerator terminals to allow their respective voltages, V_a and V_d, to be varied separately. For the case involving reaction (2), the accelerator voltage is nominally set near $V_a = V_d/2$. The potentials are measured by two precision voltage-divider strings. (See Figs. 2 and 4 of Ref. [6].) Since the accelerator and decelerator both have potentials proportional to the output of the high-voltage power supply, voltage fluctuations do not effect the energy-loss spectra. The variable-angle accelerator is pivoted about the center of the scattering chamber housing with the angular position controlled by a stepping motor rotating a precision threaded rod attached to the undercarriage of the ion accelerator. A postcollision analysis magnet is used to separate out specific charge states after the collision region. The postscattering magnet and ion-energy analyzer, which is housed in the decelerator terminal, remain stationary.

The projectile ions used in this work were produced in a commercially available electron-impact ion source manufactured by the Colutron Corporation. In order to produce ^{3}He^{2+}, the ion source had to be operated with a higher potential across the anode and filament, or discharge region, than normally required. Unfortunately, this mode of operation reduced the ion source lifetime from several days, which is typical of normal operation, to about 5 h.

The ions are extracted by a 2-kV potential and passed through an Einzel lens focusing element before entering a Wein velocity filter. The mass-selected ions then enter the main acceleration region, where a column focus and extraction system focus the incident beam onto the entrance of the scattering target. After passing through the scattering target, ions are deflected into the deceleration region by an analyzing magnet. Ions neutralized in the target region pass undeflected through the magnet and into a neutral-detector chamber. This arrangement allows simultaneous measurement of both neutral ions and charged ions resulting in the collision process.

After the ions are decelerated, they are energy analyzed by either a cylindrical or retarding-field analyzer. During the course of these experiments, we found that the cylindrical analyzer was inadequate and a retarding-field analyzer was installed. The shortcomings of the cy-

lindrical analyzer and a description of the retarding-field analyzer are presented below. A more detailed description of the operation of the apparatus is given in Refs. [6] and [7].

III. PRELIMINARY RESULTS

Figure 1 illustrates the energy levels of the He^{2+} + He system. Conservation of energy restricts kinetic-energy gain or loss values Q to

$$Q = 2[1/(n)^2 + 1/(n')^2] - I_p - 2 \text{ (a.u.)} , \qquad (5)$$

where I_p is the single-ionization energy of He (0.904 a.u.) and energy gain results in $Q > 0$. The only $Q > 0$ superelastic channel is that with $n = n' = 1$. Notice that interchange of the n and n' indices results in the same energy losses. For instance, when an electron is captured into the $n = 2$ state of the projectile and the target is left in the $n' = 1$ state, the energy loss is the same as for capture into the $n = 1$ level of the projectile with the target left in the excited $n' = 2$ level. Thus the energy loss-gain method is inadequate for extracting specific target or projectile state-selective capture cross sections from this system. Nonetheless, this method can still yield information on the superelastic channel and limited information for higher n and n' values.

Figures 2 and 3 illustrate energy loss-gain single-capture spectra, taken with the cylindrical analyzer, for ^{3}He^{2+} incident on He and Ar. For the He target, the $n = 1$ and 2 capture channels are clearly seen. Capture into the $n = 3$ and higher states was observed to be negligible. The anomalous features occurring between the $n = 1$ and $n = 2$ channels were quite reproducible, but did not correspond to any of the energy-loss-gain values of the system. A possible cause of these anomalous peaks is discussed below.
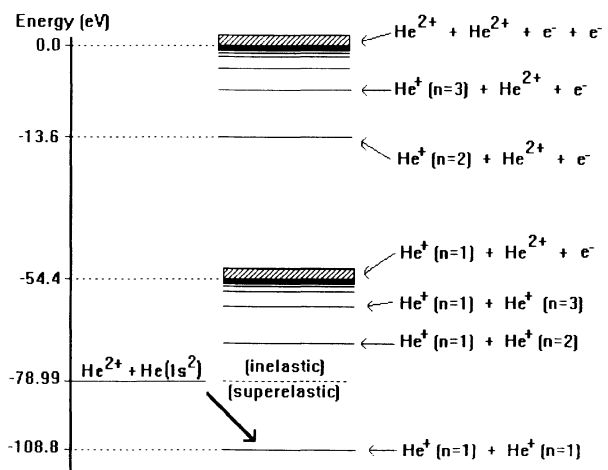

FIG. 1. Schematic diagram for the energy levels of the He and He^{2+} system. The numbers in parentheses represent particular n states. The transition pictured represents the superelastic $n = n' = 1$ capture process. The initial binding energy is 79 eV for He. The final state consists of two He$^+$ ions with a net binding energy of 108.8 eV. The difference in potential energy of the two states is converted into kinetic energy.
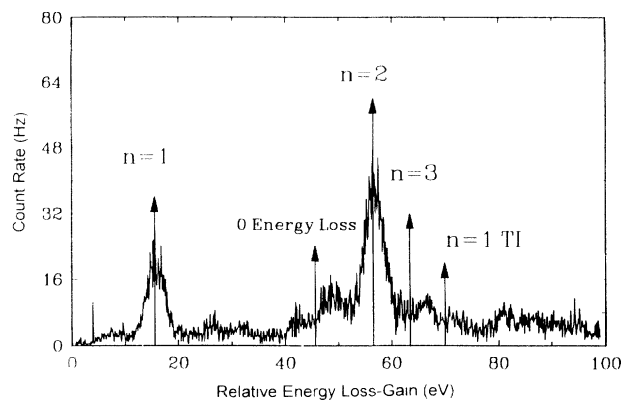
FIG. 2. Energy loss-gain spectrum of $^3He^+$ formed through collisions of 30-keV/u $^3He^{2+}$ ions incident on He. The energy gain peak labeled as $n = 1$ corresponds to superelastic scattering of the projectile $^3He^+(n = 1)$ state. The major central $n = 2$ peak corresponds to inelastic capture with either the projectile or target ion in the $n = 2$ state with the partner ion remaining in the ground state. The inelastic $n = 3$ position and transfer ionization (TI) threshold are indicated as well.

For Ar targets the superelastic $n = 1$ channel (energy gain of 38 eV) was observed to be negligible. If we assume that the cross sections for energy gain or loss processes decrease as their "energy defect," or magnitude of energy loss-gain, increases, then this is understandable qualitatively when compared to the case of He targets with an energy gain of 30 eV for the $n = n' = 1$ superelastic peak [11]. The Ar $n = 2$ and $n = 3$ TI peaks are also observed. Background spectra taken without target gas for both He and Ar had count rates less than 3 to 4 Hz.

Severe experimental difficulties were encountered in the acquisition of these energy loss-gain spectra involving the cylindrical analyzer. Due to the low $^3He^{2+}$ incident-beam currents (< 5 nA), low count rates, and short lifetime of the ion source (which was less than 5 h due to the

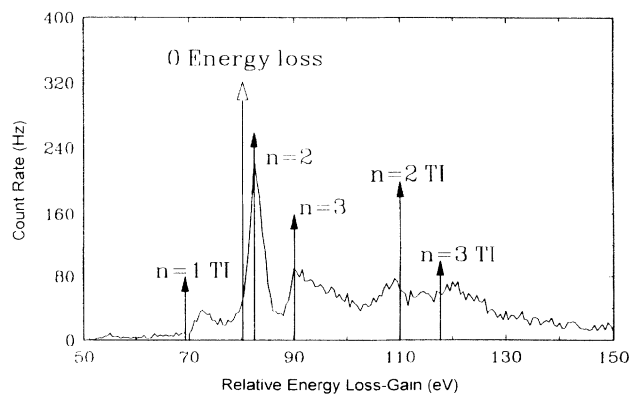FIG. 3. Energy loss-gain spectrum of $^3He^+$ formed through the collisions of 30-keV/u $^3He^{2+}$ ions incident on Ar. The superelastic capture channel for both residual ions in the ground state was observed to be negligible. Transfer ionization (TI) thresholds for capture into $n = 1$, 2, and 3 states of $^3He^+$ are also indicated.

increased power required for α particle production), it became very difficult to properly guide the product $^3He^+$ beam (≈ 1 pA) into the analyzer within the available operating time of the ion source.

Since typical count rates for He targets were on the order of 20 to 30 Hz at target pressures of 40 to 60 mTorr, pressure tests to ensure single collision conditions (which would involve pressures well below 40 mTorr) could not be done properly. Some of the anomalous features between the $n = 1$ and $n = 2$ capture positions for He targets may be attributable to multiple collisions within the scattering cell, due to the high target pressures required to see reasonable "product" signal levels. Due to the experimental difficulties encountered with the cylindrical analyzer, a retarding-field analyzer was designed, constructed, and installed in the apparatus.

IV. RETARDING-FIELD ANALYZER

Retarding-field analyzers have been used extensively to measure electron energies [12,13]. Because we are examining heavy ions instead of electrons, stray electric and magnetic fields pose less of a problem. One must also note that in the initial detector configuration of the apparatus, ion energies were already reduced to 2 keV in the decelerator before entering the cylindrical analyzer. In this sense, the deceleration section of the apparatus is already a partial retarding field analyzer (RFA).

The RFA used in this work consisted of four major components: a main deceleration region, a zoom lens drift region, a set of retarding-field grids, and, as was the case with the cylindrical analyzer, a Johnston Laboratory particle multiplier. (See Fig. 4.) After passing through the target region and switching magnet, ions that entered the main deceleration region were reduced to an energy of approximately 400 eV. Then they entered the zoom lens drift region. All lens elements were held at the decelerator potential. This provided a field-free drift region for the ions and also established a well-defined potential before the retarding fields. Since the resolution of a retarding-field analyzer depends critically on the values of momenta perpendicular to the retarding field and beam axis, an aperture was installed in the last zoom lens element to discriminate against ions with large components of perpendicular velocity. After passing through the aperture, the ions were subjected to the retarding field. A dual set of gold wire grids, which were electrically connected, provided the retarding potential. The distance between the grids was approximately $\frac{1}{2}$ inch. Ions with sufficient energy to overcome the potential barrier of the first grid drifted across the field-free region between the grids and passed through the second grid. Since the Johnston Laboratory detector was operated with the first dynode, or collector plate, at -4000 V with respect to the decelerator potential, ions exiting the second retarding grid were strongly accelerated and focused onto the detector. The high voltage applied to the detector also ensured that all ions striking the first dynode had roughly the same kinetic energy.

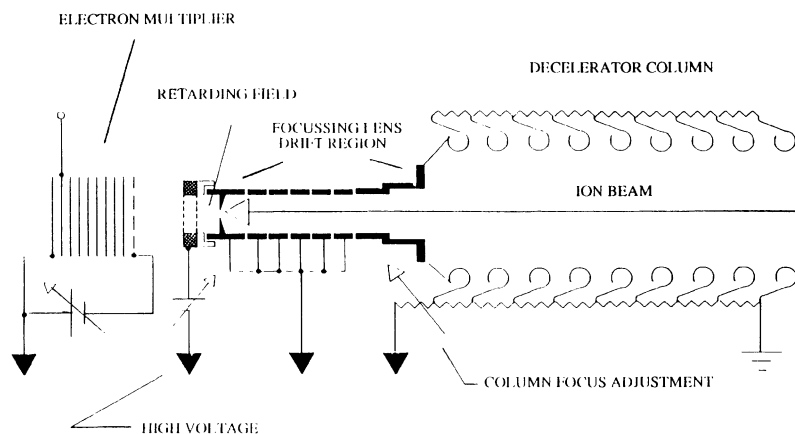Figure 5 illustrates a retarding-voltage scan of the

FIG. 4. Ion-energy retarding-field analyzer (RFA).

product ^{3}He^{+} ions produced in α-helium collisions for a projectile energy of 30 keV/u. The full ^{3}He^{+} ion beam is detected at 150 V. As the retarding voltage is increased, ions suffering from transfer ionization energy losses begin to be blocked by 210 V and the signal decreases. At 270 V, only the $n = 1$ and $n = 2$ capture channels have enough energy to overcome the retarding barrier, and when the voltage reaches 290 V, only the $n = 1$ superelastic ions remain.

In order to make a comparison with spectra obtained with the cylindrical analyzer, the spectrum in Fig. 2 was integrated and is shown in Fig. 6. One can readily see that the position and relative magnitudes of the features in both spectra agree well. If the anomalous peaks previously observed between the $n = 1$ and $n = 2$ channels were real, the slope on the retardation scans to the left of the $n = 1$ cutoff position would have a negative value. Since the measured slope is essentially zero it can be safely concluded that the anomalous features are an experimental artifact.
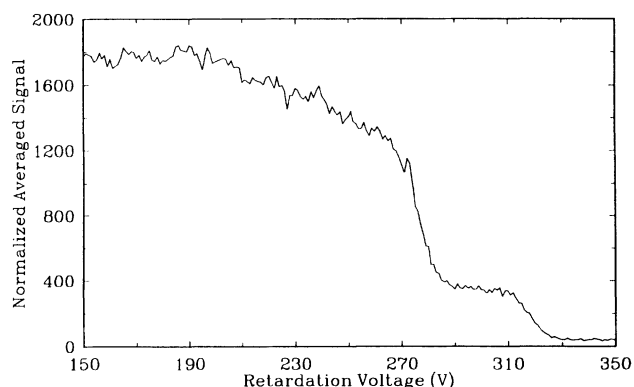
Retardation spectra were taken for Ar and Ne targets with projectile energies of 30 keV/u, and are illustrated in Figs. 7 and 8. The Ar spectrum shows that the $n = 1$ superelastic channel is negligible, while transfer ionization is enhanced, in agreement with the previous cylindrical analyzer spectra. Ionization energies for He, Ne, and Ar are 24.5, 21.6, and 15.8 eV, respectively. Since a resonant zero energy-loss capture process will occur if the binding energy of the target is equal to the 13.6-eV binding energy of the $n = 2$ level of ^{3}He^{+}, one may expect that the ratio of the $n = 1$ to $n = 2$ capture signals will be suppressed when the ionization potential of the target is near the ^{3}He^{+}($n = 2$) binding energy [11]. This is in qualitative agreement with the spectra.

Count rates with the RFA were typically in the 1000-Hz range, so pressure tests to ensure single-collision conditions could be done properly. After energy scans were taken for He targets, we recorded the retardation voltages for the $n = 1$ and $n = 2$ levels, as well as the voltage at which all ions were detected. With the RFA set at these various voltages, we then measured signal rate versus target pressure while the incident-beam current was monitored. These tests indicated that in all cases, single collision conditions were ensured for target pres-

FIG. 5. Retardation voltage spectrum of ^{3}He^{+} formed in collisions of 30-keV/u ^{3}He^{2+} incident on He. The ion signal was normalized to the measured neutral signal, which varies linearly with the incident beam for constant He target pressures. The spectrum depicted represents an average of three separate data runs. Each spectrum was first normalized to the measured ^{3}He neutral count rate, formed through double capture in the collision region. The average was then taken at each voltage and the results are plotted.
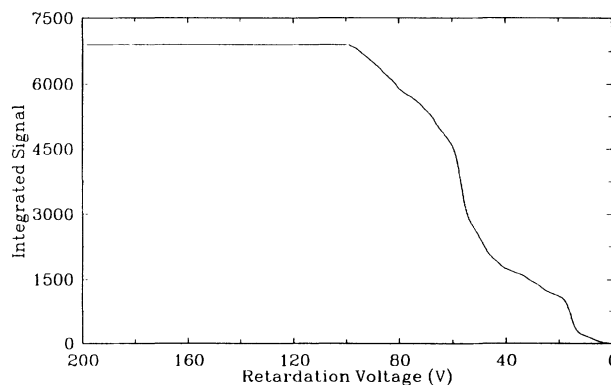

FIG. 6. Integrated energy-loss-gain spectrum from Fig. 2 (see text). Since the spectrum of Fig. 2 covered only a 100-V range, a straight line was added to simulate the rest of the spectrum. The positioning of the plotted spectrum was chosen arbitrarily for comparison
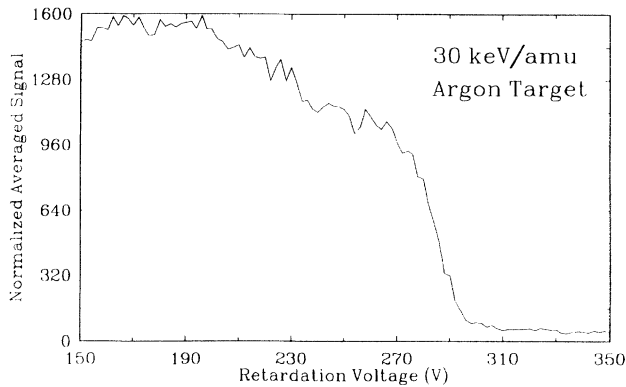
FIG. 7. Retarding-voltage spectrum of ^{3}He$^+$ formed through the collision of 30-keV/u ^{3}He^{2+} incident on argon.

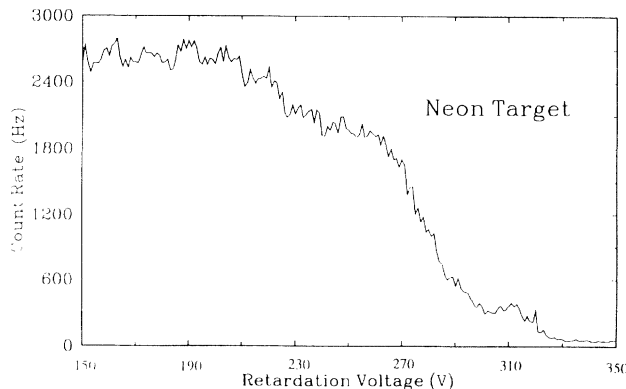FIG. 8. Retarding-voltage spectrum of ^{3}He$^+$ formed through the collision of 30-keV/u ^{3}He^{2+} incident on neon.
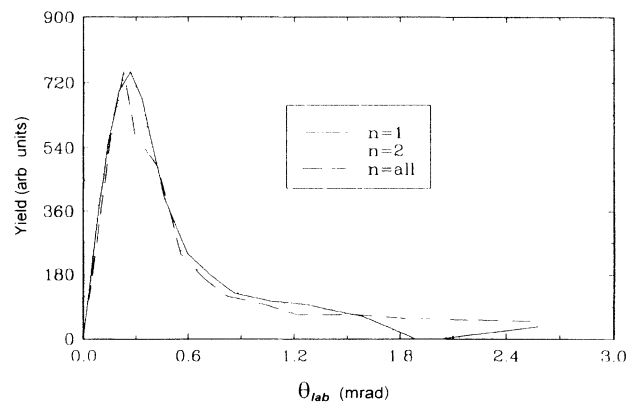

FIG. 9. Angular spectra for 15-keV/u incident projectile energy. The maximum heights of the $n = 1$ and $n = 2$ capture channels were normalized to that of the $n =$ all (where all ions are detected) capture signal after multiplying by $\sin\theta$. (See text.)

sures below 40 mTorr. Subsequent data runs involved target pressures between 15 and 20 mTorr.

Angular scans of the features in the retardation spectra were made at all energies. Since the individual n-state contributions to the total cross section are obtained by integrating $\sin\theta \, d\sigma/d\Omega$ over the full angular range, a true indication of the "weight" with which a given value of $d\sigma(\theta)/d\Omega$ contributes to the total cross section is obtained by plotting $\sin\theta \, d\sigma(\theta)/d\Omega$ versus θ. Plotting the data in this way has the additional benefit that details of the functional dependence on θ of $d\sigma/d\Omega$ are made more apparent at large angle, where they would normally be obscured by the small values of $d\sigma/d\Omega$. Thus, each angular spectrum was multiplied by $\sin\theta$. Figure 9 illustrates typical angular scans at 15 keV/u after normalizing the $n = 1$ and $n = 2$ spectral maxima to the maximum of the spectrum obtained when all ions were detected. As the results indicate, the angular dependence of all observable capture channels were essentially the same. This means that the relative state-selective capture cross sections at a given energy can be obtained from single-angle ($\theta = 0°$) retardation spectra alone, without integrating over scattering angle.

V. RESULTS AND CONCLUSIONS

In order to extract relative cross sections from the raw data, all RFA voltage spectra were background corrected, smoothed, and differentiated. Each derivative spectrum was then used to determine the maximum retardation voltage V_1 corresponding to complete transmission of the $n = 1$ superelastic ions. After the $n = 1$ and $n = 2$ peaks were located in the derivative spectrum, the maximum voltage position V_1 between the $n = 1$ and $n = 2$ peaks, in which the derivative became zero, was recorded. In some cases the derivative never reached zero, so the maximum voltage at which a minimum occurred was used. Ten data points were taken from the corresponding undifferentiated spectrum ranging from $(V_1 - 20 \text{ V})$ to V_1 and were averaged. Since the $n = 2$ level is exactly 40.8 eV from the $n = 1$ capture channel, the count rate of the $n = 2$ level was taken at a retarding voltage position of $V_1 - 40.8$. To obtain an average total ion count rate in which all ^{3}He$^+$ ions were detected, all data points ranging from the lowest retardation voltage measured to the highest voltage at which the ion signal first began to decrease were averaged. The relative cross sections ob-

TABLE I. Final state-selective single-electron-capture results for ^{3}He^{2+} incident on He. The designation $n = 1$ and $n = 2$ signifies electron capture into the $n = n' = 1$ and either the $n = 2$, $n' = 1$ or $n = 1$, $n' = 2$ states, respectively. Uncertainties given represent relative error. Overall error due to normalization to the data of Refs. [8] and [9] is about 22%.

Energy (keV/u)	$n = 1$ (10^{-17} cm^2)	$n = 2$ (10^{-16} cm^2)
15	4.46±0.16	0.884±0.035
30	6.89±0.26	1.50±0.06
45	5.64±0.24	1.45±0.06

tained in this manner were then put on an absolute scale by normalizing to the total single-capture and transfer ionization data of Shah, McCallion, and Gilbody [8] and Dubois [9]. The results are given in Table I. The uncertainties presented in Table I represent the standard deviation of the mean of all repeated measurements. Nonstatistical fluctuations, for which we have no immediate explanation, occurred in most data sets. Nonetheless, relative uncertainties were always below 5% of the cross-section values.

Figure 10 compares the final results to the experimental data of Afrosimov et al. [10] and good agreement is seen where the data overlap. Since Afrosimov's data is the sum of the $n = 2$, 3, and 4 capture levels, we expect that our cross sections for $n = 2$, $n' = 1$ should be slightly less than their value, and this is found to be the case. As our data show, capture into the higher $n = 3$ and 4 levels is negligible for the higher energies. Calculations of the cross section for the $n = 1$ channel by the impact-parameter method obtained by Fulton and Mittleman [14] are also shown. The calculations utilized wave functions for only three states: $[He^{2+}+He(1s^2)]$, $[He(1s^2)+He^{2+}]$, and $[He^+(1s)+He^+(1s)]$. They are in good agreement with experiment. (These are the only theoretical calculations we are aware of for this system.)

From the experimental cross sections measured for He targets, and examination of the spectra for Ne and Ar, it appears that electrons are preferentially captured into n levels that have binding energies close to that of the single-ionization potential of the target. In addition, the closer the ionization potential of the target is to the $n = 2$ binding energy of He^+, the more diminished the $n = 1$ superelastic channel becomes. For hydrogen targets, the ionization potential is exactly equal to that of the $n = 2$ state of He^+. Thus one may predict that the superelastic
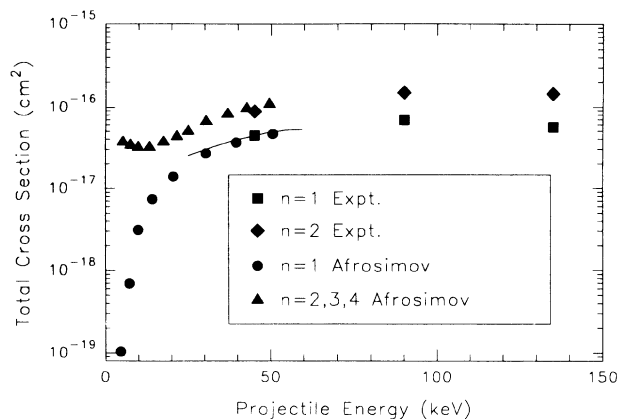

FIG. 10. Total state-selective capture cross sections for $^3He^{2+}$ incident on He. Relative errors are less than 5%. Overall errors are about 22% due to normalization to data of Shah, McCallion, and Gilbody [8] and of Dubois [9]. Solid line indicates theoretical calculations of Fulton and Mittleman [14] utilizing the impact-parameter method.

$n = 1$ capture channel will be greatly diminished for hydrogen targets, with capture occurring predominantly into the "resonant" $n = 2$ state.

ACKNOWLEDGMENT

[1] T. F. Stratton, Plasma Diagnostic Techniques, edited by R. H. Huddlestone and S. L. Leornard (Academic, New York, 1965).

[2] J. T. Park, J. M. George, J. L. Peacher, and J. E. Aldag, Phys. Rev. A 18, 48 (1978).

[3] J. T. Park, J. E. Aldag, J. M. George, and J. L. Peacher, Phys. Rev. A 14, 608 (1976).

[4] J. E. Aldag, J. L. Peacher, P. J. Martin, V. Sutcliffe, J. M. George, E. Redd, T. J. Kvale, D. M. Blankenship, and J. T. Park, Phys. Rev. A 23, 1062 (1981).

[5] J. T. Park, and F. D. Schowengerdt, Rev. Sci. Instrum. 40, 753 (1969).

[6] T. J. Gay, V. D. Irby, and S. P. Yallaly, Rev. Sci. Instrum. 64, 1644 (1993).

[7] V. D. Irby, Ph.D. thesis, University of Missouri–Rolla, 1992.

[8] M. B. Shah, P. McCallion, and H. B. Gilbody, J. Phys. B 22, 3037 (1989).

[9] R. D. Dubois, Phys. Rev. A 36, 2585 (1987).

[10] V. V. Afrosimov, A. A. Basalaev, G. A. Leiko, and M. N. Panov, Zh. Eksp. Teor. Fiz. 74, 1605 (1978) [Sov. Phys. JETP 47, 837 (1978)].

[11] R. E. Olson (private communication).

[12] J. A. Simpson, Rev. Sci. Instrum. 32, 1283 (1961).

[13] T. Gimpal and O. Richardson, Proc. R. Soc. London, Sect. A 182, 17 (1943).

[14] M. J. Fulton and M. H. Mittleman, Proc. Phys. Sci. 87, 669 (1966).